Guiding Wi-Fi Sensor Placement for Enhanced CSI-Based Sensing in Stationary Crowd Counting

He Wang, *Student Member, IEEE,* Jingtao Guo, *Student Member, IEEE,* and Ivan Wang-Hei Ho, *Senior Member, IEEE*

***Abstract*—Recent studies in Wi-Fi sensing have demonstrated the potential of channel state information (CSI) for indoor crowd counting. However, their practical application remains limited by constraints in sensing range and robustness. While multi-transceiver setups have shown promise in enhancing performance, the impact of transceiver placement strategies on sensing effectiveness remains underexplored. In this work, we systematically investigate how sensor placement affects sensing performance in stationary crowd counting. We extend two foundational models, the Fresnel zone and sensing-signal-to-noise ratio (SSNR) formulations, originally designed for single-target, single-link scenarios, and generalize them to characterize spatial sensing quality in multi-target, multi-link environments. Based on this theoretical foundation, we propose a deployment evaluation model that quantifies sensing performance using a normalized metric termed the Regional Sensing Quality (RSQ), and enables direct comparison among different transceiver topologies. Experimental results across diverse environments show that optimizing deployment can improve crowd counting accuracy by up to 20.48%, with our system achieving 98.14% accuracy for up to 20 individuals. This work provides the first framework that integrates theoretical modeling and practical validation to guide transceiver deployment for robust and scalable CSI-based stationary crowd sensing.**

***Index Terms*—Wi-Fi sensing, channel state information (CSI), Multi-sensors, Placement, Crowd counting.**

I. Introduction

In the past decade, researchers have revealed the untapped potential of Wi-Fi for sensing applications beyond its conventional role in wireless communication, leading to renewed research and innovation in this area. The foundation of Wi-Fi sensing lies in the principle that channel state information (CSI) derived from Wi-Fi signals exhibits variations in response to target movements [1]. These signal variations can be analyzed to extract valuable information about the context of the target, including parameters such as speed and displacement. CSI-based contactless sensing has attracted significant attention due to its low-cost nature, non-intrusiveness, and preservation of privacy [2], [3]. Its potential applications are vast, including Human Activity Recognition (HAR), fall detection, crowd counting, and vital sign monitoring in healthcare [4]–[6]. Most prior efforts have focused on algorithmic improvements, with limited attention to the physical configuration of transceivers, which plays a crucial role in determining the sensing performance of such systems.

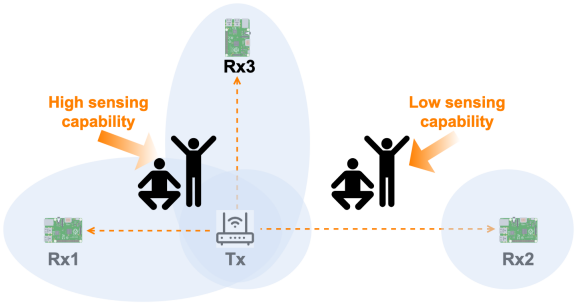

Fig. 1. Impact of transceiver placement on sensing capability in a multi-target environment.

Although Wi-Fi-based sensing has been applied to a wide range of tasks, most studies emphasize algorithmic innovations while relying on fixed or heuristic transceiver placements. In single-target applications, prior works have noted that device placement affects signal behavior, which can be explained using the Fresnel zone or sensing coverage models [7]–[9]. However, these insights are generally confined to simplified, single-link configurations. Recent advances in multi-link CSI sensing aim to improve scalability and robustness through the use of multiple transceivers [10], [11], but they often adopt randomized layouts without systematic evaluation or generalizable design strategies. These limitations are especially critical in multi-target applications such as stationary crowd counting, as depicted in Fig. 1, which illustrates how transceiver placement affects sensing quality. However, many existing studies in this area focus on enhancing model performance through signal processing or learning-based techniques [5], [12], [13], and only a few have considered how physical deployment factors, such as transceiver height or Line-of-Sight (LoS) and Non-Line-of-Sight (NLoS) conditions, affect sensing accuracy [14], [15]. These works typically analyze isolated parameters and lack a unified framework for evaluating the impact of the transceiver placement in realistic, multi-target, multi-link scenarios.

To bridge this gap, we systematically analyze how transceiver placement affects spatial sensing quality in multi-target scenarios by combining geometric intuition from the

This work was supported in part by the Smart Traffic Fund (Project No. PSRI/31/2202/PR) established under the Transport Department of the Hong Kong Special Administrative Region (HKSAR), China.

The authors are with the Department of Electrical and Electronic Engineering, The Hong Kong Polytechnic University, Hong Kong (e-mail: edana.wang@connect.polyu.hk; jingtao2023.guo@connect.polyu.hk; ivanwh.ho@polyu.edu.hk).

Fresnel Zone model with a region-level evaluation model that quantifies sensing quality via a metric termed the Regional Sensing Quality (RSQ). Rather than relying on exhaustive search, our model enables quantified comparison among feasible topologies under real-world constraints. As illustrated in Fig. 1, we validate this framework in stationary crowd counting, an ideal use case for evaluating multi-target sensing capabilities across diverse deployment strategies. We specifically address the following research questions:

1) Can the Fresnel zone model and sensing coverage model, previously applied to single-target applications, be extended to support multi-target applications?
2) Does the optimal distance phenomenon, as demonstrated in prior studies for single-link scenarios [7], [16], still hold under multi-link scenarios?
3) Can a generalizable sensing capability model be developed for multi-link Wi-Fi sensing, similar to those used in diverse multi-sensor networks [17]?
4) How do spatial target distributions affect sensing performance in multi-link scenarios, and can we propose a model to guide the selection of effective deployment topologies?

To address these questions, we conducted experiments in typical indoor environments for stationary crowd counting, such as a meeting room and a double-decker bus. By systematically evaluating the impact of target-transceiver distance, transmitter-receiver separation, and multi-sensor placement, we aim to enhance sensing performance in real-world scenarios. Our objective is to develop a systematic framework that models, evaluates, and guides transceiver placement strategies for CSI-based stationary crowd counting. This framework bridges theoretical modeling with practical deployment validation, enabling high-quality sensing and supporting scalable deployment across diverse environments. The key contributions of this study are three-fold.

1) We extend two foundational models, originally developed for single-target scenarios, to guide transceiver deployment in stationary crowd counting. The Fresnel Zone model captures placement sensitivity to target distribution via diffraction and reflection, while the SSNR-Based evaluation model quantifies region-level sensing quality in multi-target, multi-link environments. To our knowledge, this is the first work to integrate both for deployment guidance.
2) We propose a deployment evaluation model to compare and select optimal transceiver topologies for stationary crowd counting. The model quantifies sensing quality over spatial regions using the RSQ metric, enabling objective assessment of deployment effectiveness across diverse target distributions and indoor geometries. Validated against empirical results across various scenarios, it serves as a generalizable and scalable tool for guiding sensor placement in real-world environments.
3) We conduct comprehensive experiments to assess the impact of deployment strategies guided by our proposed model. In a controlled indoor setting, optimizing transceiver distances and topologies based on our SSNR-based scoring function improves crowd counting accuracy by 11.75% and 6.14%, respectively. In a real-world deployment on a double-decker bus, our optimized placement combined with data fusion achieves a 20.48% gain over the baseline.

The rest of this paper is organized as follows. Section II reviews related work and Section III introduces the fundamental technique and model of CSI-based sensing. An overview of the crowd counting system is provided in Section IV, followed by the presentation of implementation and evaluation results of the stationary counting system in Section V. Lastly, Section VI discusses the conclusion and future works based on the findings in this paper.

II. Related Work

A. CSI-based Crowd Counting

Crowd counting has garnered significant attention across a variety of CSI-based sensing applications in the research landscape. CSI-based crowd counting systems in the literature are typically classified into two primary types based on target motion: i) Dynamic, where targets move randomly within the venue, and ii) Static, where targets are expected to remain seated but can engage in activities like eating, typing, or talking. Previous studies have predominantly focused on estimating the number of moving individuals in settings such as meeting rooms, offices, or laboratories [18], [19]. These studies emphasize participant movement, noting decreased accuracy when individuals are stationary [15]. However, numerous real-world scenarios involve stationary individuals, like library readers or passengers on public transport. Counting stationary individuals presents challenges due to reduced signal variations. Recent models have started addressing stationary scenarios [5], [12], [20], yet accuracy in counting a large number of stationary individuals remains limited, with a capped countable limit of 15 individuals [5]. To enhance scalability, multiple wireless links has been proposed as a potential solution [12].

B. Device Placement

Device positioning has recently attracted research interest within the wireless sensing community, alongside signal processing strategies and hardware design [21]. Two prevalent model-based placement approaches exist for a single pair of transceivers. The first is the Fresnel zone model, which explains how the performance of CSI-based applications is affected by target locations, as described by the Fresnel zone theory [22]. This theory has been validated across various single-target applications. Sensor placement strategies are guided by Fresnel zone theories, with different models recommended for targets situated inside and outside the FFZ [23]. Wang et al. [8] utilized the reflection model, designating the area within the FFZ as ineffective. Bocus et al. [24] explored three device placement topologies based on target locations: Line-of-Sight (LoS), 90 degrees, and adjacent. Their results highlighted the superior performance of the LoS configuration, with a combination of all three placements yielding the lowest

performance due to differing Doppler signatures between LoS and non-LoS setups.

The second model is the sensing coverage model introduced in [7], which suggests that the sensing capacity of a Wi-Fi system is influenced by the distances between transceivers and the target. As the distance between Tx and Rx increases, the sensing coverage area initially expands but eventually contracts. With a fixed distance between Tx and Rx, the sensing capacity relative to the target's position forms a Cassini oval. This model has been validated and applied in various CSI-based applications [25], [26]. However, all the aforementioned works utilize a single-target single-link sensing application. There remains a gap in the literature regarding device placement models in multi-link scenarios for multi-target applications.

C. Multi-sensor Strategies

In multi-link scenarios, two key considerations are sensor placement topologies and data fusion strategies. While existing models have addressed device placement with a single pair of transceivers, placement becomes more complex in multi-sensor environments, particularly in terms of improving scalability and minimizing interference among multiple transceivers. Wang et al. [8] explored four placement topologies and showed that recognition accuracy improves with uniformly spaced sensor pairs and a greater number of transceivers. Similar findings are reported in cross-link tracing systems using one transmitter and multiple receivers [27]. However, existing literature lacks a generalizable methodology for selecting optimal multi-sensor topologies, which this work seeks to address.

Another crucial aspect in multi-sensor systems is the choice of data fusion strategies. Fusion methods generally fall into three categories: majority voting, where each link is processed independently and final decisions are made via voting [28]; likelihood fusion, which aggregates class-wise likelihoods across links [29], [30]; and feature fusion, which concatenates or transforms features from multiple links before classification [31]. In our study, we implement both feature and likelihood fusion for comparative evaluation.

III. Preliminary

In this section, we present the foundational models and introduce our proposed evaluation framework for Wi-Fi sensing. We begin by generalizing two classic models: the CSI model and the Fresnel Zone model. Building on the SSNR-based sensing formulation, we then propose a region-level evaluation model that quantifies spatial sensing quality via the RSQ metric. As the core of our framework, this RSQ-based model is complemented by Fresnel-based geometric intuition to guide transceiver placement in stationary crowd counting.

A. CSI Model

CSI serves as a comprehensive representation of the channel state, encompassing propagation effects such as scattering, fading, and multipath. It provides an estimation of the channel

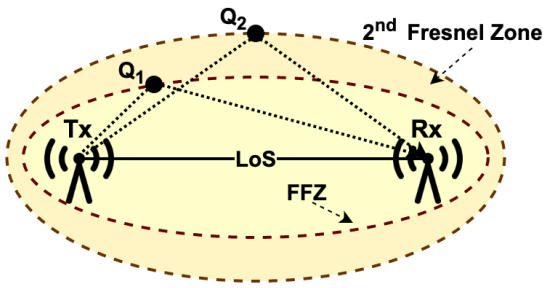

Fig. 2. Illustration of the Fresnel zone reflection model.

coefficients, which capture the impulse or frequency response at the subcarrier level. In indoor environments, walls and human bodies cause signal reflections, leading to multipath propagation at the receiver. These paths can be categorized into static paths, which encompass the LoS path and reflections from stationary objects, and dynamic paths, which arise due to changes in target objects, such as human motions. CSI is utilized to characterize the channel between the Tx and Rx in Wi-Fi systems. The received signal at the receiver can be mathematically represented as

$$Y(f,t) = H(f,t) \times X(f,t), \tag{1}$$

where $X(f,t)$ and $H(f,t)$ represent the frequency domain representations of the transmitted signal and the complex-valued channel frequency response (CFR) at a specific carrier frequency f and time t.

The CSI matrix can be expressed as a linear combination of all the reflected paths, formulated as

$$\begin{aligned} H(f,t) &= H_s(f,t) + H_d(f,t) + H_n(f,t) \\ &= |H_s(f,t)|\, e^{-j\theta_s} + |H_d(f,t)|\, e^{-j\theta_d} \\ &+ |H_n(f,t)|\, e^{-j\theta_n}, \end{aligned} \tag{2}$$

where H_s, H_d, and H_n denote the contributions from the static path, dynamic path, and noise, respectively, and $|H|$ and θ represent the amplitude and phase of each CSI component.

In orthogonal frequency-division multiplexing (OFDM) systems, the frequency spectrum is divided into numerous subcarriers that are transmitted concurrently. As a result, the CSI varies across different subcarriers while maintaining a certain degree of correlation. If N packets and S subcarriers are recorded, the resulting CSI matrix can be represented as

$$H = \begin{bmatrix} h_{1,1} & h_{1,2} & \dots & h_{1,S} \\ h_{2,1} & h_{2,2} & \dots & h_{2,S} \\ \vdots & \vdots & \vdots & \vdots \\ h_{N,1} & h_{N,2} & \dots & h_{N,S} \end{bmatrix}, \tag{3}$$

where $h_{i,j}$ denotes the CSI value corresponding to the jth subcarrier at the ith packet.

B. Fresnel Zone Model

Previous studies have validated the applicability of the Fresnel zone model for a wide range of sensing applications

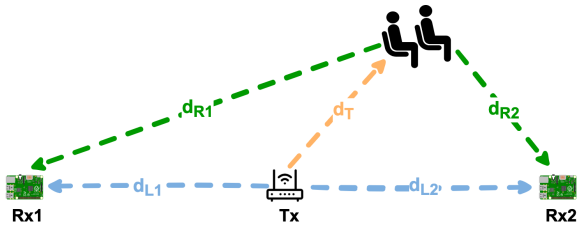

Fig. 3. Sensing model with multiple sensors.

in indoor environments [4], [23]. A layout of the Fresnel zone is illustrated in Fig. 2, where two-dimensional ellipses are utilized for clarity instead of the actual three-dimensional ellipsoids. Fresnel zones are defined as concentric ellipses with a pair of transceivers serving as the foci. For simplicity, we denote the positions of the transceivers as Tx and Rx, and represent the distance between them as $|T_xR_x|$. Given a specific radio wavelength λ, the Fresnel zone can be constructed as

$$|T_xQ_n| + |R_xQ_n| - |T_xR_x| = \frac{n\lambda}{2}, \tag{4}$$

where n represents the number of concentric ellipses and Q_n denotes a point within the n^{th} ellipse. The signal path length of a reflected or diffracted signal that traverses the boundary of the n^{th} Fresnel zone is extended by $\frac{n\lambda}{2}$ relative to the LoS path signal.

Research has indicated the significance of the first ten Fresnel zones in RF transmission, with over 70% of the signal energy being transmitted through the FFZ [32]. As a target moves into the FFZ, diffraction becomes notably stronger and emerges as the dominant factor. Conversely, as the target moves out of the FFZ, reflection becomes the primary mechanism. For targets located either inside or outside the FFZ, different models should be applied for CSI-based sensing. In our system, the design of the topology must consider that individuals are positioned beyond the FFZ to effectively utilize the Fresnel reflection model. According to [33], the maximum diameter of the FFZ can be calculated as

$$F_1 = \sqrt{\frac{cD}{f}}, \tag{5}$$

where c is the speed of light, D is the distance between the transceivers, and f is the radio frequency. For a frequency of 5 GHz and a distance of 10 m, the maximum diameter of the FFZ is calculated to be 0.77 m. When the distance between the transceivers is reduced to 5 m, the maximum diameter of the FFZ decreases to approximately 0.55 m.

While the FFZ calculation defines its geometric size, it does not directly determine the sensing coverage. Rather, the Fresnel zone model is used to characterize signal propagation behaviors (e.g., diffraction vs. reflection) and guide transceiver placement strategies. By analyzing device, target, and environmental factors, it helps interpret how these factors affect sensing performance. In this study, we conducted experiments to validate its applicability to stationary crowd counting.

C. Multi-Sensor SSNR-Based Sensing Capability Model

Building on the sensing coverage model proposed in [14], we construct an SSNR-based model to characterize the sensing capability of multiple sensors in indoor environments. Fig. 3 illustrates a typical scenario with one transmitter and two receivers. The signals reflected by the target and arrived at the receivers can be categorized into two paths: i) the signal from the Tx that is reflected by the target and received by receiver 1 (Rx1), and ii) the signal that is reflected by the target and received by receiver 2 (Rx2).

The distances from the target to two receivers are denoted as d_{R1} and d_{R2}, respectively. We also define the distance between Tx and Rx1 as d_{L1}, the distance between Tx and Rx2 as d_{L2}, and the distance from Tx to the target as d_T. By applying the Friis transmission equation [34]–[36] to a single path (Tx→Target→Rx), we can derive the signal power arriving at one of the receivers as

$$P_d = \frac{P_T G_T \sigma A_R}{(4\pi)^2 (d_T d_R)^2}, \tag{6}$$

where P_T represents the transmission power, G_T indicates the antenna gain of the transmitter, and σ represents the radar cross section (RCS) of the target, which encompasses the effective reflection ratio at the target [37]. The term A_R corresponds to the effective aperture of the receiver's antenna, which can be calculated as $A_R = \frac{G_R \lambda^2}{4\pi}$, where G_R represents the antenna gain of the receiver and λ signifies the wavelength of the signal.

A metric known as sensing-signal-to-noise ratio (SSNR) was introduced by Wang et al. [7] to quantify sensing capability:

$$SSNR = \frac{P_d}{P_i} = \frac{P_d}{\gamma P_s + b}, \tag{7}$$

where P_d represents the power of the dynamic signal, and P_i denotes the interference power, which is linearly proportional to the static power P_s. The constants γ and b capture hardware-dependent interference scaling. While Wang et al. [7] introduced them empirically, they can be treated as fixed values for a given transceiver pair. The static path is assumed to be the LoS path, which can be mathematically expressed as

$$P_s = \frac{P_T G_T A_R}{4\pi (d_L)^2}. \tag{8}$$

Since each receiver can filter packages solely from the transmitter, we can calculate the SSNR for each receiver individually. Substituting (6) and (8) into (7), and denoting the combined constant $K = \frac{P_T G_T A_R}{4\pi}$, we obtain the $SSNR$ expression for a single target:

$$SSNR = \frac{P_d}{\gamma P_s + b} = \frac{K\sigma}{(4\pi)(d_T d_R)^2 (\gamma \frac{K}{d_L^2} + b)}, \tag{9}$$

where the transmission power P_T, antenna gains G_T and G_R, and signal wavelength λ are assumed to be constant. Assuming a constant RCS of the target σ and a small value for b, (9) can be simplified as

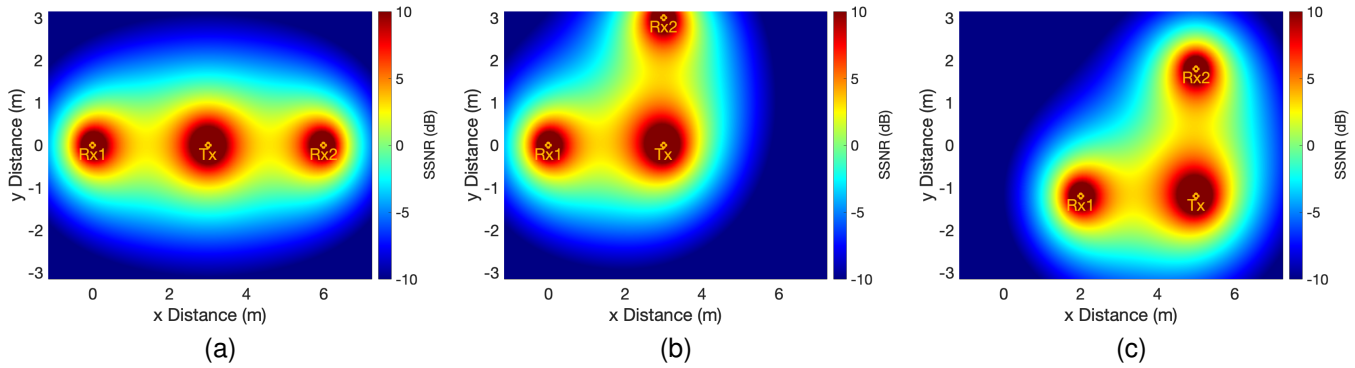

Fig. 4. Heatmap of sensing capability with various topologies. (a) 180 degrees. (b) 90 degrees case 1. (c) 90 degrees case 2.

$$SSNR \propto \frac{d_L^2}{(d_T d_R)^2}. \tag{10}$$

To extend the SSNR model to a multi-receiver setting, we consider the contributions from multiple Tx–Target–Rx paths. We assume that these paths are conditionally independent and that their signal contributions are additive in terms of expected energy. For example, with two receivers, the combined SSNR becomes:

$$SSNR_{comb} \propto \frac{d_{L1}^2}{(d_T d_{R1})^2} + \frac{d_{L2}^2}{(d_T d_{R2})^2}. \tag{11}$$

The derived equation illustrates the intricate connection between sensing capability and different distances, specifically the distances among multiple transceivers. As the transceivers vary in position, both the sensing capability and coverage undergo changes. The sensing capability of the proposed model under a few realistic options for sensor placement is depicted in Fig. 4.

A larger SSNR value indicates a higher sensing capability. As depicted in Fig. 4, the sensing capability increases when targets are in close proximity to the devices and decreases as targets move farther away. The analysis also indicates that the shape of the sensing coverage area is impacted by the placement of multiple sensors. The topology shown in Fig. 4a is more suitable for a rectangular room, while Fig. 4b and Fig. 4c are more suitable for triangle or square rooms. Based on the observation, the sensing capability and optimal topology vary depending on the distance between the Tx and the Rx, as well as the distance between the targets and transmitters.

D. Evaluation Model for Stationary Crowd Counting

In previous sections, we introduced the SSNR formulation for multiple sensors to assess the sensing capability of a single target. Existing studies, such as [7], utilize a minimum SSNR threshold to delineate the sensing boundary and optimize transceiver distance. However, in stationary crowd counting where multiple targets coexist across the space, each location produces a different SSNR, so a fixed minimum SSNR threshold cannot accurately define a joint sensing boundary for all targets.

Moreover, exhaustive optimization of transceiver positions is infeasible in typical indoor deployments due to layout constraints and limited device counts. To address these challenges, we propose a lightweight SSNR-based evaluation model that computes a region-level scoring function, referred to as RSQ, to quantify the expected sensing quality over a designated area (by default, the entire indoor environment), and enables direct comparison among a set of practically feasible deployment strategies.

We first discretize the target region into a 2D grid with 0.3 m resolution, where each grid point represents a potential target position. The SSNR at each point is computed by aggregating the signal strength from all transceiver pairs, based on the model proposed in Section III-C. For a transceiver deployment consisting of one transmitter and N receivers, the SSNR at grid point P is defined as:

$$SSNR(\mathbf{p}) = \sum_{i=1}^{N} \frac{d_{L,i}^2}{(d_{T,i} \cdot d_{R,i})^2}, \tag{12}$$

where $d_{L,i}$ is the distance between the transmitter t and the i-th receiver r_i, $d_{T,i}$ is the distance from the transmitter to point P, and $d_{R,i}$ is the distance from the receiver to point P. The SSNR value at each point is converted to the logarithmic scale (dB) to better reflect perceived signal differences. The average SSNR over the target region Γ is then given by:

$$\mu_{\text{dB}} = \frac{1}{|\Gamma|} \sum_{\mathbf{p}_j \in \Gamma} 10 \cdot \log_{10}(SSNR(\mathbf{p}_j)), \tag{13}$$

where $|\Gamma|$ is the total number of grid points within the target region, and $\mathbf{p}_j \in \Gamma$ denotes the location of the j-th grid point in the region. We then map the average SSNR in dB to a region-level sensing quality score in the range [0, 1], termed RSQ, using a scaled sigmoid function:

$$RSQ = \frac{1}{1 + \exp(-(\alpha \cdot \mu_{\text{dB}} + \gamma))}. \tag{14}$$

In this work, the parameters α = 0.7 and γ = 3.71 are calibrated by fitting the function to SSNR-RSQ pairs from representative deployments, ensuring a practical sensitivity range for stationary crowd counting.

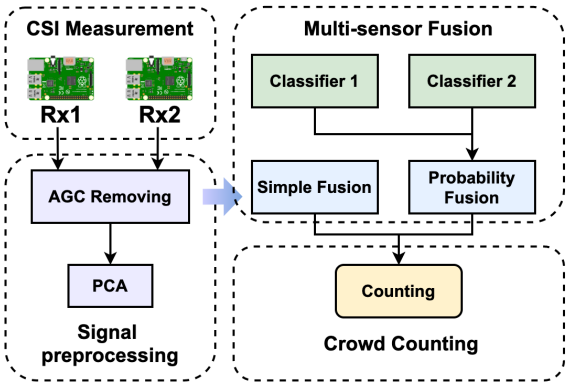

Fig. 5. Crowd counting system framework.

The proposed evaluation model extends SSNR from a point-wise metric to a region-wide evaluation criterion. Specifically, it aggregates the SSNR values over a designated target region and maps the average SSNR into RSQ ranging from 0 to 1. This metric enables comparative evaluation of a small number of feasible deployment strategies, making it particularly practical for real-world Wi-Fi sensing scenarios, including stationary crowd counting. In Section V, we further validate this evaluation model and demonstrate its applicability in both single-link and multi-link scenarios.

IV. Crowd Counting System Overview

Our system is designed to count the number of stationary individuals in indoor environments or passengers on public transportation. It can be implemented using either single or multiple sensor topologies. The framework of our system is illustrated in Fig. 5, which encompasses four modules detailed as follows.

A. CSI Measurement

The system employs a passive data collection method in monitor mode using the Nexmon CSI Extraction Tool [38]. This approach minimizes hardware and power requirements compared with active collection methods, such as the Linux 802.11n CSI Tool [39], which require the transmitter to send dedicated signals to the receiver. In this passive setup, receivers capture existing Wi-Fi data frames from an AP without injecting traffic or modifying protocols, ensuring full compatibility with standard network operations. To maintain a high and stable sampling rate (1 kHz) required for real-time sensing, an auxiliary Raspberry Pi periodically sends lightweight ping packets to the router, generating a consistent packet stream for CSI extraction [40]. This introduces only minor additional traffic and does not disrupt normal Wi-Fi connectivity.

Similar passive configurations with auxiliary traffic generation have also been adopted in prior works using Nexmon [6], [41], [42], and have been shown to enable high-rate CSI extraction while preserving communication integrity.

B. Signal Preprocessing

CSI data collected using the Nexmon CSI Tool is often quite noisy [40] and requires further preprocessing. Due to the significant noise introduced by carrier frequency offset (CFO) and sampling frequency offset (SFO), we focused exclusively on the amplitude component of the received CSI in this system. To enhance performance, we eliminated 14 null subcarriers, resulting in a total of 242 subcarriers for an 80 MHz bandwidth. The following two preprocessing steps are applied to the CSI data:

1) CSI Calibration: The original CSI extracted from the receiver is affected by the automatic gain control (AGC), which distorts amplitude and limits the sensing coverage to approximately 2-4 meters due to environmental variations and human movements [43]. To address this, we reverse the AGC process using a calibration method based on received signal strength (RSS) [44]. This calibration process rescales the CSI amplitude from a broad range to a range between 0 and 1, thereby bolstering the resilience of our system against environmental variations.
2) CSI Feature Extraction: Principal Component Analysis (PCA) is employed to identify correlations among CSI streams, which reflect changes due to body movements. We discovered that although the first PCA component is typically deemed as noise [45], it actually contains valuable information, contrary to certain prior studies [46]. By analyzing the ratio of retained information across dimensions, we determined that retaining 119 dimensions maintains 99.9% of the information, leading to a reduction in the input size for a single receiver by about 50.83%. This dimensionality reduction substantially lowers computational complexity and training duration while upholding accuracy.

C. Multi-sensor Fusion

As mentioned in Section II-C, we executed two distinct fusion methods tailored for multi-sensor scenarios. The first method, labeled “Simple Fusion” and illustrated in Fig. 5, entailed combining the CSI data gathered from the two receivers. To maintain consistency in input size comparable to the single-receiver scenario, we utilized the PCA method for dimensionality reduction and feature extraction.

The second fusion method, termed “Probability Fusion”, utilizes the predicted probabilities of each class derived from previously trained machine learning models for each receiver. These predicted probabilities (e.g., 7-class distributions from each receiver) are concatenated to form a 14-dimensional input vector for the fusion model. We use a Random Forest (RF) classifier to learn from this fused input and produce the final crowd count prediction. The final count is determined by selecting the class with the highest predicted probability from the fusion classifier.

D. Crowd Counting

The output generated by the multi-sensor fusion process will become input in the crowd counting model. This paper

emphasizes the enhancements provided by multiple sensors and their corresponding topologies; therefore, we employed conventional machine learning techniques, including support vector machines (SVM), RF, and K-nearest neighbors (KNN), to train the passenger counting classifiers and to compare the performance across different scenarios. Although deep learning methods could further improve accuracy [47], their implementation may diminish the significant distinctions among various strategies. We utilized a five-fold cross-validation approach, in which the CSI data is divided into five subsets. One subset is designated as the test data, while the remaining four are used for training the model. Accuracy is defined as the proportion of correctly classified samples in the test set for each fold. This process is repeated five times, and the overall system performance is assessed by averaging the results from all five iterations.

V. Implementation and Evaluation

This section presents a comprehensive evaluation of placement factors that influence the performance of stationary crowd counting. Through systematic variation of parameters under diverse conditions, we aim to verify the effectiveness of theories proposed in Section III on stationary crowd counting and to answer the questions proposed in Section I. These insights will then be utilized to design optimized topologies for passenger counting applications within the context of double-deck buses.

A. Implementation

This study utilized the Nexmon CSI Extraction Tool, compatible with the Raspberry Pi platform [38], to collect CSI data for stationary crowd counting. The tool supports up to 80 MHz bandwidth with 802.11a/g/n/ac transmissions in both the 2.4 and 5 GHz bands. To optimize information capture, 80 MHz bandwidth in the 5 GHz band was employed, resulting in 242 subcarriers after null removal. CSI data packets were stored in a pcap file format for subsequent processing in Python or Matlab. Raspberry Pi 4B devices were utilized as receivers, each set to channel 36 and filtered using the nexutil command [38]. A Huawei WS7002 router was chosen as the AP for its cost-effectiveness and compact design. Each Raspberry Pi, equipped with a single antenna and Wi-Fi chip, captured a single CSI matrix. A sampling frequency of 1 kHz was applied to collect CSI data across different scenarios.

B. Evaluation Setup

In this study, a comprehensive experimental investigation was carried out in a meeting room measuring 8.4 m $\times$ 6.3 m. In the meeting room setup, both the Tx and Rx were placed on adjustable tripods at a height of 1 meter above the ground. Specific transceiver placements varied across experimental conditions and are detailed in Sections V-C and V-D. The experiments involved up to six participants (two females and four males), aged between 24 and 28. Each experimental scenario included three trials, with the seating positions of participants randomized in each trial to minimize bias and ensure the validity of the results. To ensure comparability across scenarios, the quantity of targets and seating positions remained consistent, facilitating a direct contrast of outcomes among different scenarios. The research systematically examined the impact of the Fresnel zone model and the sensing capability model on the accuracy of stationary crowd counting. Building upon these results, the study delved into optimizing sensor placement strategies to enhance sensing capability by incorporating multiple sensors. Additionally, the theoretical insights obtained were utilized in designing topologies for passenger counting in a double-deck bus setting, where two receivers were used to count up to 20 passengers. In this setting, devices were mounted to the ceiling using adhesive mounts, at an approximate height of 1.75 meters above the floor. The specific transceiver placements depended on the experimental topology and are described in Section V-E.

C. Evaluation with a single link

1) Exploring the effect of the First Fresnel zone: In this subsection, we first examine the signal amplitude characteristics when all participants are either inside or outside the FFZ. Then, we investigate how mixing signals from both regions affects counting accuracy in multi-person setups.

In the first experiment, individuals were positioned in a specific arrangement: first, all were seated inside the FFZ, and subsequently, all were seated outside it, forming a row that reflects a common seating layout in real-world scenarios. Experimental results demonstrate a significant variation in CSI amplitude based on human presence within and outside the FFZ. As depicted in Fig. 6, in the absence of individuals, CSI amplitude remains relatively constant. However, when individuals are positioned within the FFZ, a decrease in CSI amplitude is observed compared to when they are seated outside the FFZ. This reduction in amplitude within the FFZ suggests a decrease in signal power, likely attributed to signal diffraction within this region. It is noteworthy that not all subcarriers exhibit this pattern. Some subcarriers demonstrate a higher CSI amplitude inside the FFZ than outside. Nevertheless, given the consistent pattern observed across the majority of subcarriers, an average across the 242 subcarriers was calculated using a Savitzky-Golay filter [48] to illustrate this phenomenon.

These findings align with previous research [8], which reported a significant drop in CSI amplitude when a single individual was located inside the FFZ during HAR. However, such single-target studies do not encounter the model mismatch issue that arises in stationary crowd counting. In multi-target environments, individuals may be simultaneously positioned both inside and outside the FFZ, causing the CSI signals to combine effects from different physical mechanisms—namely diffraction and reflection. This mixing of signal propagation models introduces challenges for feature extraction, potentially degrading counting accuracy in multi-person scenarios.

To investigate this phenomenon, we designed two contrasting experimental configurations, illustrated in Fig. 7. In the mixed scenario, participants were placed both within and outside the FFZ, whereas in the comparison scenario, all

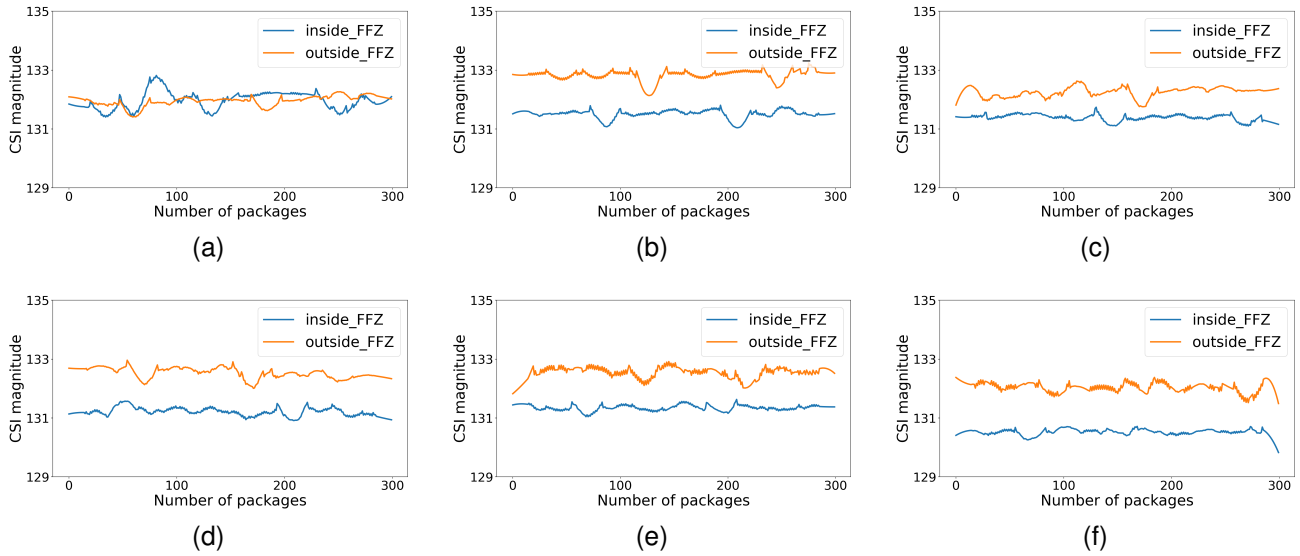

Fig. 6. Comparison of the amplitude of the CSI inside and outside the FFZ. (a) Empty. (b) 1 person. (c) 2 persons. (d) 3 persons. (e) 4 persons. (f) 5 persons.

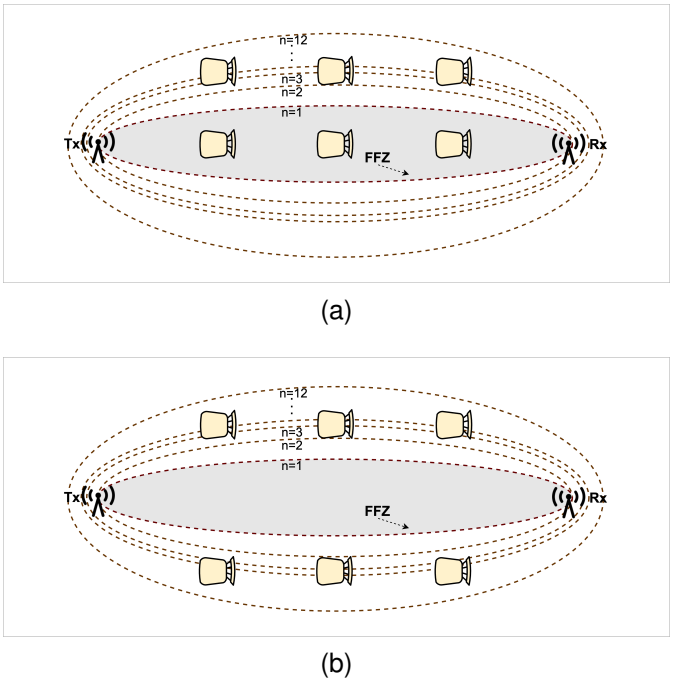

Fig. 7. Experiment setup in two conditions. (a) Sitting inside and outside of the FFZ. (b) Sitting outside of the FFZ.

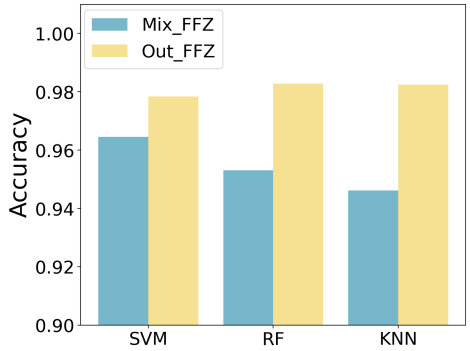

Fig. 8. Evaluation results of the effect of the First Fresnel zone on crowd counting.

participants were situated outside the FFZ. This setup enabled a direct comparison of counting accuracy when merging data from various regions against a scenario using data solely from outside the FFZ.

The experimental results, as shown in Fig. 8, reveal a consistent trend in counting accuracy. Blue bars depict accuracy in the mixed scenario (participants within and outside the FFZ), while yellow bars show accuracy in the comparison scenario (all participants outside the FFZ). Regardless of the training methods employed, the accuracy achieved when all participants are situated outside the FFZ consistently surpasses the accuracy obtained in the mixed scenario. Particularly notable is the KNN method, where the accuracy of the mixed scenario decreased by 3.64%. One potential explanation for this phenomenon could be that the diffraction and reflection models respectively characterize the relationship between signal variations and target movements when the target is located inside and outside the FFZ [23]. This finding supports the initial hypothesis that integrating CSI data from within and outside the FFZ may reduce counting accuracy. Moreover, these results reinforce that while the Fresnel Zone model offers valuable geometric intuition and is best suited for single or closely grouped targets, it does not generalize well to distributed-target scenarios. In contrast, the RSQ evaluation model provides a scalable and quantitative framework for assessing sensing quality across diverse deployments.

2) Exploring the effect of the distance between the transceivers and targets: To complement the above analysis, this subsection isolates the effect of participant location by comparing uniform configurations: all participants inside or outside the FFZ. Unlike the previous experiment, this avoids signal-model mixing and focuses on how spatial distance from

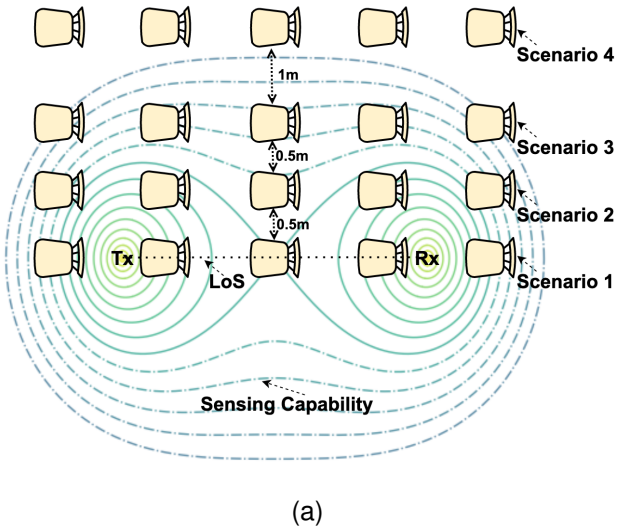

(a)

Fig. 9. Experiment setup in four scenarios.

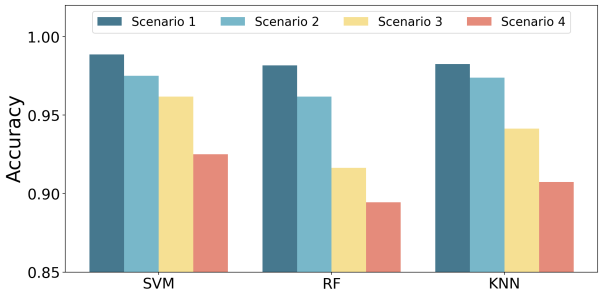

Fig. 10. Evaluation results of the effect of the device-target distance.

the transceivers influences counting accuracy. Specifically, the distance between the Tx and Rx was set at 5 meters. Data collection involved varying numbers of participants (0 to 5) across different configurations, as shown in Fig. 9.

- Scenario 1: All participants were positioned in a line within the LoS and within the FFZ.
- Scenario 2: Participants were positioned in a line at a distance of 0.5 m from the LoS.
- Scenario 3: Participants were positioned in a line at a distance of 1 m from the LoS.
- Scenario 4: Participants were positioned in a line 2 m away from the LoS, significantly further from the FFZ.

The experimental design aims to validate the proposed evaluation model and examine the relationship between sensing capability and the distance between transceivers and targets. In our evaluation model, the sitting positions across the four scenarios are represented as four rectangular target regions, each with a length of 5 m and a width of 0.5 m. According to the model introduced in Section III-D, the calculated RSQ for Scenarios 1 through 4 are 0.993, 0.960, 0.889, and 0.153, respectively, demonstrating a clear degradation in sensing quality as the distance between transceivers and targets increases.

Fig. 10 presents the accuracy results, revealing a consistent pattern across all models. In Scenario 1, where participants are positioned within the FFZ, the highest accuracy is consistently

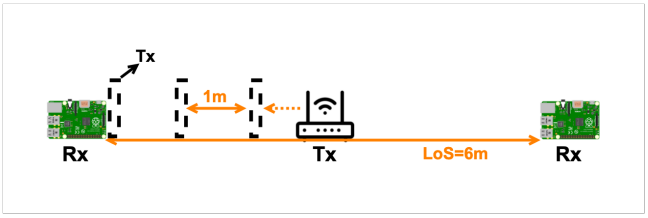

Fig. 11. Experiment setup for various Tx-Rx distance.

achieved. Accuracy decreases as participants are positioned farther from the transceivers, aligning with the evaluation model and theoretical insights described in Section III-C and III-D. This phenomenon is primarily attributed to signal power dynamics. Over 70% of signal energy is transmitted via the FFZ, with diffracted signals exhibiting greater strength than reflected signals, especially when targets are within the FFZ. As radio signals attenuate in air, reflected signals weaken with distance, and the sensing quality may degrade significantly when participants are located far from the transceiver pair. These results demonstrate that the proposed evaluation model remains effective for assessing sensing quality in single-link, multi-target scenarios.

D. Evaluation with multiple links

1) Exploring the effect of the distance between the Tx and Rx with multiple sensors: This experiment examines the influence of the distance between multiple sensors on crowd counting accuracy, expanding on prior research that pinpointed an optimal distance for enhancing coverage range and performance in wireless sensing applications [7], [16]. The study delves into the impact of different distances between multiple sensors, with the aim of determining the most effective distance for accurate crowd counting in multi-sensor scenarios.

To simplify the experiment, two receivers were positioned 6 meters apart, with a single transmitter placed in the middle (Fig. 11). We moved the position of the transmitter so that the distance between the transmitter and one receiver was systematically varied from 0 to 3 meters (in 1-meter increments), while for the other receiver, it was varied from 6 to 3 meters. Participants (0 to 5) were randomly placed within the sensing coverage area, ensuring they remained outside the FFZ. According to the proposed evaluation model, the RSQ for these four asymmetric-to-symmetric transceiver layouts is 0.545, 0.608, 0.684, and 0.712, respectively, indicating improved sensing quality as the deployment becomes more balanced. This experimental setup enables the examination of counting accuracy under different distances between multiple sensors, contributing to the development of appropriate topologies for crowd counting applications in the case of multiple sensors.

To evaluate the effectiveness of the optimal distance in multiple sensor scenarios, two fusion methods, as described in Section IV-C, were applied to process data collected from different receivers. The results, presented in Fig. 12, show that both the simple fusion (blue bars) and probability fusion

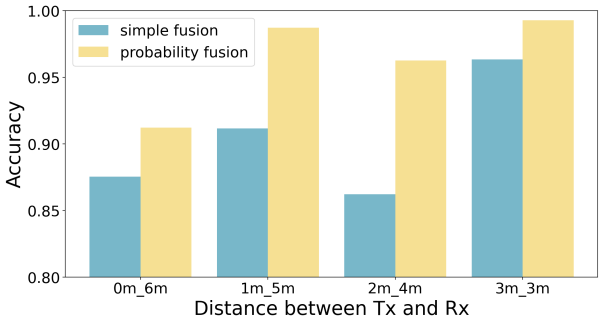

Fig. 12. Evaluation results of the effect of the Tx-Rx distance on multiple sensors.

(yellow bars) methods achieved the highest accuracy when the distance between each transceiver was 3 m. The label of each bar indicates the distance between the Tx and each Rx. In both methods, the accuracy achieved by the optimal distance is 11.75% and 8.85% higher than in the non-ideal scenarios. These results confirm that the optimal distance principle holds true in multi-sensor deployments and highlight the importance of balanced topology design. This consistency with the proposed evaluation model further supports its practical utility in guiding effective transceiver placement for stationary crowd counting.

2) Exploring the effect of various topologies in general on crowd counting: To evaluate the effect of various topologies on the performance of crowd counting, we collected data under the same settings, except for the device deployment. The experiment enabled flexible transceiver placement at various angles and positions, with a focus on realistic configuration scenarios. In Fig. 13, three topologies were designed based on two common spatial patterns observed in real-world environments: 1) The transmitter is placed at the center of the room, while the receivers are positioned along the boundaries, as illustrated in Fig. 13a and Fig. 13b. The difference in receiver positions in these two figures result in varying angular arrangements between the transceivers. 2) As shown in Fig. 13c, the transmitter is placed in a corner of the room, while the relative distance between transceivers is maintained consistent with that in Fig. 13b. The locations of various targets are indicated as triangles in Fig. 13, representing five volunteers seated in different configurations. The colors of these triangles correspond to the theoretical model shown in Fig. 4, where orange indicates higher sensing capability, followed by green and blue. As summarized in Table I and based on the sensing quality evaluation model proposed in Section III-D, we expect that, in this rectangular environment, the 180-degree topology will offer the highest sensing capability across all positions within the room, with a computed RSQ of 0.712. This is followed by Case 2 of the 90-degree topology with an RSQ of 0.531 and then Case 1 with a lower RSQ of 0.497.

The accuracy results of this experiment are displayed in Fig. 14. The variations among these three topologies are more pronounced in the simple fusion method (blue bars), while the probability fusion method (yellow bars) achieves an accuracy higher than 99% in all scenarios. Generally, the topology with a 180-degree configuration performs better than the 90-degree setup in this environment, showing an improvement of 4.76% with simple fusion. For the 90-degree cases, positioning the midpoint between the two receivers at the center of the room achieves higher accuracy compared to placing the Tx at the center, with an improvement of 3.82% through simple fusion. These results are consistent with the sensing quality predicted by the proposed evaluation model. This further validates the model's ability to reflect the real-world sensing performance of different transceiver configurations.

3) Exploring the effect of target positions on crowd counting: Besides the location of devices, the position of targets also affects the selection of optimal topologies. In this experiment, we will verify the impact of target locations on the performance of various topologies. We mainly compared two scenarios: 1) targets located throughout the entire space; and 2) targets concentrated in the upper half of the space, especially near the left side of the room. According to the proposed sensing quality evaluation model and our previous experiments, when volunteers are distributed across the entire area, the topology with 180 degrees achieves better performance. However, when considering only the upper half of the area, the 90-degree topology demonstrates a higher sensing capability, with an RSQ of 0.786, compared to 0.712 for the 180-degree layout. This is because more signal power is concentrated in the left-upper region under the 90-degree configuration, as shown in Table I.

The accuracy results are shown in Fig. 15. When volunteers are located throughout the entire space, the topology with 180 degrees achieves high accuracy for both the simple fusion method (blue bars) and the probability fusion method (yellow bars), with a maximum improvement of 6.14%. However, in the scenario where volunteers are located only in the upper half of the room, the 90-degree topology performs better compared to the 180-degree topology, improving by 3.17%. These results are consistent with the sensing quality evaluation model proposed in Section III-D, confirming that the optimal transceiver topology is dependent on the spatial distribution of the targets.

This study emphasizes the critical factors that influence the performance of crowd counting utilizing multiple sensors. Strategic placement and topology design necessitate careful consideration of target, Tx, and Rx positions. Minimizing the mixing of targets within and outside the FFZ by controlling the positions of the Tx and Rx is crucial for accurate counting. Sensing capability enhancement can be achieved by deploying sensors in proximity to targets and maintaining a balanced optimal distance between transceiver pairs.

These findings provide actionable insights for real-world sensor placement in Wi-Fi-based sensing applications. The proposed evaluation model offers a practical and generalizable approach to quantifying sensing quality across different deployment strategies, thereby facilitating informed and efficient design decisions. Beyond stationary crowd counting, this model can be extended to other multi-target sensing scenarios.

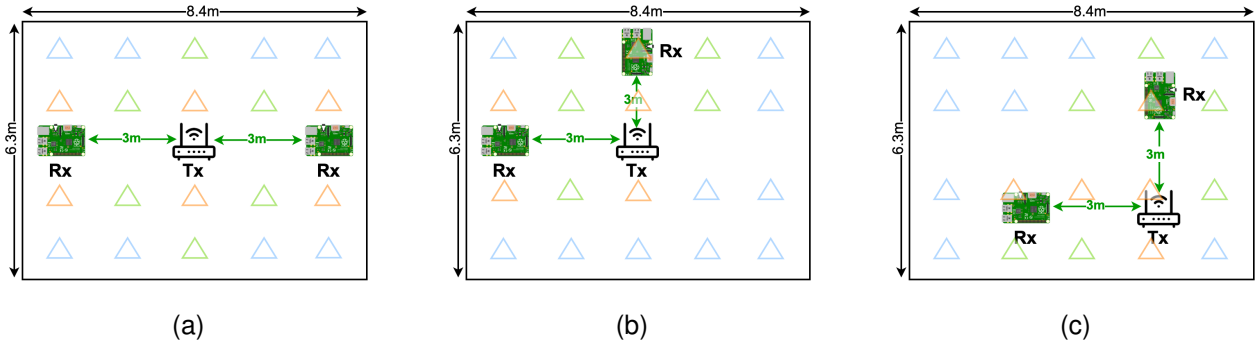

Fig. 13. Sitting positions in a meeting room. (a) 180 degrees. (b) 90 degrees case 1. (c) 90 degrees case 2.

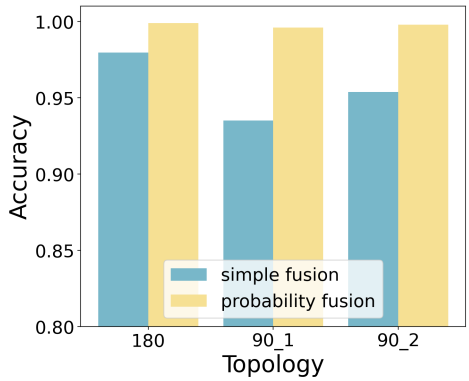

Fig. 14. Evaluation results of the effect of various topologies on crowd counting.

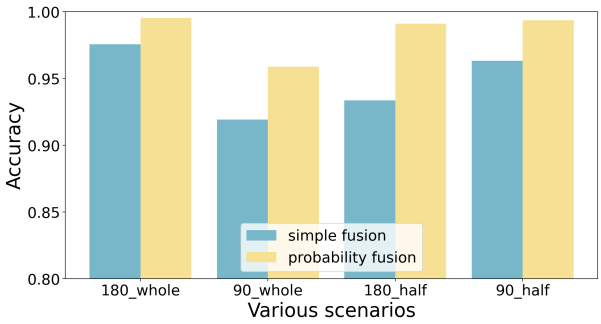

Fig. 15. Evaluation results of the effect of target positions with various topologies on crowd counting.

TABLE I
ACCURACY AND RSQ OF VARIOUS CASES

Topologies	Simple fusion	Probability fusion	RSQ
180	97.97%	99.90%	0.712
90_1	93.52%	99.60%	0.497
90_2	95.38%	99.79%	0.531
180_half	93.36%	99.10%	0.712
90_half	96.32%	99.37%	0.786

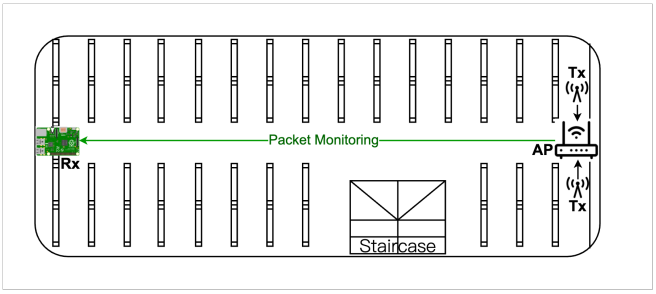

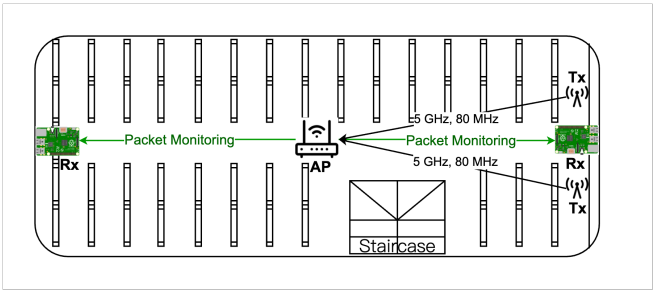

Fig. 16. Layout of the upper deck of the double-deck bus. (a) Topology 1. (b) Topology 2.

E. Evaluation on a double-deck bus

To demonstrate the practical applicability of our sensor deployment strategies in a realistic environment, we conducted experiments on the upper deck of a double-decker bus. To ensure reliable data collection, the bus remained stationary throughout the trials. This reflects common real-world scenarios in which passenger counting is performed when the bus is stopped, such as at stations or red lights. The configuration of the bus deck is depicted in Fig. 16. The upper deck features a total of 53 seating positions arranged in 15 rows, with an inter-column spacing of approximately 0.64 meters. The internal dimensions of the upper deck measure approximately 10.71 meters in length, 2.38 meters in width, and 1.75 meters in height. These spatial parameters are significant factors influencing signal propagation and the potential for multipath interference within the experimental setting.

TABLE II
ACCURACY AND RSQ OF CANDIDATE BUS TOPOLOGIES

Topologies	Simple fusion	Probability fusion	RSQ
tp2_1	95.14%	99.19%	0.991
tp2_2	94.02%	99.97%	0.978
tp2_3	94.15%	99.99%	0.982
tp3	95.22%	100%	0.995
tp4	95.24%	100%	0.999

1) Model-guided evaluation of candidate topologies in bus scenario: We first conduct experiments using various receiver topologies based on the layout of the upper deck of the bus. To minimize the impact of device deployment on passengers, all receivers are positioned along the edges or in the corners of the ceiling. To validate the generality of the proposed SSNR-based deployment evaluation model in the bus scenario, we collect data under each topology configuration with four passengers, simulating a low-density but spatially distributed crowd. We then compare the RSQ and the corresponding crowd counting accuracies across several candidate multi-link topologies, in which the Tx is consistently placed at the center of the ceiling on the upper deck.

- tp2_1: Two Rxs are placed at the center positions of the front and rear sides of the upper deck.
- tp2_2: Two Rxs are placed on the same side of the front and rear ends of the upper deck.
- tp2_3: Two Rxs are placed diagonally at the front and rear corners of the upper deck.
- tp3: Three Rxs are placed at three of the four corners of the upper deck.
- tp4: Four Rxs are placed at all four corners of the upper deck.

The accuracy results are presented in Table. II. Since the probability fusion approach yields accuracies exceeding 0.99 across all topologies, we primarily focus on the simple fusion results for comparative analysis. As shown, topologies tp2_1, tp3, and tp4 achieve higher accuracy than tp2_2 and tp2_3. According to the proposed evaluation model, the corresponding RSQ for tp2_1, tp2_2, tp2_3, tp3, and tp4 are 0.991, 0.978, 0.982, 0.995, and 0.999, respectively. Although tp3 and tp4 yield slightly higher RSQ and comparable accuracy, their increased hardware cost and deployment complexity make them less suitable for practical use in real-world bus environments. Among the three two-receiver configurations, tp2_1 offers the best trade-off between sensing performance and implementation feasibility. It demonstrates the highest sensing quality both theoretically and empirically, and is therefore selected for the subsequent high-density validation experiment.

2) Application of selected topology in high-density bus scenario: As the most suitable topology has been identified under a low-density setting, this experiment aims to evaluate the improvement it provides over a baseline topology in a high-density bus scenario. In this setup, CSI data was collected and analyzed with up to 20 passengers on board. Two distinct topologies were strategically deployed to enable a comparative assessment of passenger counting performance.

1) Topology 1 (tp1): This topology served as a baseline for comparison, utilizing a single receiver. A layout of tp1 is shown in Fig. 16a. According to the evaluation model, this topology achieves an RSQ of 0.778.
2) Topology 2 (tp2): Based on the insights gained from the evaluation model and previous experiments conducted in a meeting room setting, this topology deployed two strategically positioned receivers at the front and rear of the upper deck, as illustrated in Fig. 16b. A single transmitter (Huawei AP) was utilized for data collection, with two additional Raspberry Pi 4Bs employed in both topologies to facilitate data flow. The design of tp2 incorporated several key considerations:
   - FFZ Avoidance: Transceivers were strategically positioned to avoid passengers occupying the FFZ, which in this context encompassed the bus corridors.
   - Evaluation Model–Guided Topology Design: Two receivers and a transmitter are deployed in a linear topology. According to the proposed evaluation model, this configuration yields the highest RSQ (0.991) among all two-Rx candidates and is therefore considered most suitable for deployment in the bus compartment.
   - Balanced Tx-Rx Distance: The distance between the transmitter and each receiver was carefully balanced to ensure consistent signal strength and maximize the sensing capability.

TABLE III
ACCURACY RESULTS OF TOPOLOGIES WITH VARIOUS ML METHODS

Models	tp1	tp2	
		simple fusion	probability fusion
SVM	81.46%	90.83%	**98.14%**
RF	79.34%	86.31%	97.02%
KNN	74.40%	87.97%	97.70%

By utilizing a combination of different machine learning methods and fusion techniques, we obtained accuracy results for the passenger counting system on the upper deck of the double-deck bus. A detailed overview of the results obtained from each machine learning method and fusion technique is illustrated in Table III.

The comparative analysis of passenger counting accuracy between Topology 1 and Topology 2, involving up to 20 passengers, reveals a significant improvement in performance for Topology 2 using both simple and probability fusion methods. Among the three machine learning models (SVM, RF, and KNN) assessed in the simple fusion approach, SVM achieved the highest accuracy of 90.83%. However, the probability fusion method exhibited a substantial increase in accuracy, reaching 98.14% when combining the predicted probability from the RF model with the SVM fusion model. The fusion of data from both receivers consistently yields higher accuracy than using a single receiver, achieving a 20.48% relative improvement compared to the single-receiver baseline. These results align with the RSQ (0.991 for tp2 vs. 0.778 for tp1),

TABLE IV
ACCURACY AND RSQ FOR DIFFERENT BUS REGIONS UNDER DEPOT AND ROAD SCENARIOS

Region	Bus Depot	Road	RSQ
front	93.34%	87.52%	0.970
middle	97.73%	97.42%	0.997
rear	93.77%	90.75%	0.977

further validating the effectiveness of model-guided deployment design. Overall, the findings highlight the advantages of integrating multiple receivers and selecting sensing topologies based on the proposed evaluation model, leading to significant improvements in stationary crowd counting accuracy in complex environments such as double-decker buses.

3) Experimental Validation across Bus Regions and Environments: To further validate the generality of the proposed RSQ metric, we conducted additional experiments by dividing the bus into regions and comparing depot versus real-road scenarios. Specifically, the upper deck was divided into three sub-regions (front, middle, and rear) to assess regional sensing quality. Moreover, we compared two environments: (i) a bus depot rooftop parking area, simulating five stop events, and (ii) five consecutive bus stops along a real urban route in Hong Kong, where the bus remained stationary for approximately one minute at each stop. Each trial involved up to ten passengers, with a few randomly boarding or alighting at each stop.

As summarized in Table IV, the reported accuracy values correspond to the average performance of three conventional classifiers (SVM, RF, and KNN) under the simple fusion setting, providing a representative measure. The results across the three regions are consistent with the RSQ predictions, with the middle region achieving the highest accuracy and sensing quality. Furthermore, the depot and road experiments yield comparable performance, indicating that the proposed RSQ evaluation model remains valid across both controlled and real-world bus environments. These findings confirm that the observed accuracy trends remain stable across different stationary scenarios, thereby addressing potential concerns about environmental interference or vehicle placement.

VI. CONCLUSION AND FUTURE WORK

This paper presents a unified framework for optimizing sensor placement in CSI-based Wi-Fi sensing systems, aiming to enhance the capability and scalability in multi-target environments. Our contributions lie in three key aspects: (1) a Fresnel zone-based understanding of signal propagation, (2) an SSNR-based spatial sensing capability model, and (3) a novel region-level deployment evaluation model that quantifies sensing quality under real-world constraints. Together with extensive experimental validation across diverse scenarios, including a controlled indoor environment and a public transportation setting, this framework reveals crucial insights into the effects of transceiver positioning, pairwise distances, and interference mitigation strategies. It highlights the importance of proximity to targets, strategic avoidance of destructive interference zones, and balanced topology design, providing principled guidance for future wireless sensing deployments.

While our study focuses on stationary crowd counting, the proposed evaluation framework is adaptable to other tasks such as gesture or activity recognition. Future work could extend the scoring model by incorporating motion dynamics and angular sensing range to better support such applications. Moreover, we will explore more complex topologies and account for complex indoor factors like furniture layout and wall materials to further improve deployment robustness. Overall, this work offers a generalizable and theoretically grounded foundation for optimizing sensing-oriented deployments, with implications across smart homes, healthcare, and broader IoT applications.

REFERENCES

[1] Z. Yang, Z. Zhou, and Y. Liu, "From rssi to csi: Indoor localization via channel response," *ACM Computing Surveys (CSUR)*, vol. 46, no. 2, pp. 1–32, 2013.

[2] Y. Ma, G. Zhou, and S. Wang, "Wifi sensing with channel state information: A survey," *ACM Comput. Surv.*, vol. 52, no. 3, Jun. 2019.

[3] C. Chen, G. Zhou, and Y. Lin, "Cross-domain wifi sensing with channel state information: A survey," *ACM Comput. Surv.*, vol. 55, no. 11, pp. 1–37, 2023.

[4] J. Liu, W. Li, T. Gu, R. Gao, B. Chen, F. Zhang, D. Wu, and D. Zhang, "Towards a dynamic fresnel zone model to wifi-based human activity recognition," *Proc. ACM Interact. Mob. Wearable Ubiquitous Technol. (UbiComp)*, vol. 7, no. 2, Jun. 2023.

[5] H. Jiang, S. Chen, Z. Xiao, J. Hu, J. Liu, and S. Dustdar, "Pa-count: Passenger counting in vehicles using wi-fi signals," *IEEE Trans. Mobile Comput.*, vol. 23, no. 4, pp. 2684–2697, 2023.

[6] P. Kontou, S. B. Smida, and D. E. Anagnostou, "Contactless respiration monitoring using wi-fi and artificial neural network detection method," *IEEE J. Biomed. Health Inform.*, vol. 28, no. 3, pp. 1297–1308, 2023.

[7] X. Wang, K. Niu, J. Xiong, B. Qian, Z. Yao, T. Lou, and D. Zhang, "Placement matters: Understanding the effects of device placement for wifi sensing," *Proc. ACM Interact. Mob. Wearable Ubiquitous Technol. (UbiComp)*, vol. 6, no. 1, pp. 1–25, 2022.

[8] F. Wang, W. Gong, and J. Liu, "On spatial diversity in wifi-based human activity recognition: A deep learning-based approach," *IEEE Internet Things J.*, vol. 6, no. 2, pp. 2035–2047, 2018.

[9] M. G. Moghaddam, A. A. N. Shirehjini, and S. Shirmohammadi, "The effect of sensor placement in a cooking activity recognition system," in *Proc. IEEE International Instrumentation and Measurement Technology Conference (I2MTC)*, 2024, pp. 1–6.

[10] L.-H. Shen, A.-H. Hsiao, F.-Y. Chu, and K.-T. Feng, "Time-selective rnn for device-free multiroom human presence detection using wifi csi," *IEEE Trans. Instrum. Meas.*, vol. 73, pp. 1–17, 2024.

[11] N. Bahadori, J. Ashdown, and F. Restuccia, "Rewis: Reliable wi-fi sensing through few-shot multi-antenna multi-receiver csi learning," in *Proc. IEEE 23rd International Symposium on a World of Wireless, Mobile and Multimedia Networks (WoWMoM)*, Jun. 2022, pp. 50–59.

[12] B. Korany and Y. Mostofi, "Counting a stationary crowd using off-the-shelf wifi," in *Proc. ACM Int. Conf. Mobile Syst. (MobiSys)*, 2021, pp. 202–214.

[13] S. Lei, Z. Sun, Z. Yu, Z. Wang, and B. Guo, "Crowdfi: A communication efficient multi-device wi-fi sensing system," in *Proc. Int. Conf. Mobile HCI (MobileHCI)*, 2023, pp. 1–7.

[14] X. Ma, W. Xi, X. Zhao, Z. Chen, H. Zhang, and J. Zhao, "Wisual: Indoor crowd density estimation and distribution visualization using wi-fi," *IEEE Internet Things J.*, vol. 9, no. 12, pp. 10 077–10 092, 2021.

[15] H. Hou, S. Bi, L. Zheng, X. Lin, Y. Wu, and Z. Quan, "Dasecount: Domain-agnostic sample-efficient wireless indoor crowd counting via few-shot learning," *IEEE Internet Things J.*, vol. 10, no. 8, pp. 7038–7050, 2022.

[16] H. Wang, Y. Ge, and I. W.-H. Ho, "Wall-proximity matters: Understanding the effect of device placement with respect to the wall for indoor wi-fi sensing," 2025. [Online]. Available: https://arxiv.org/abs/2412.13208

[17] B. Wang, "Coverage problems in sensor networks: A survey," *ACM Comput. Surv.*, vol. 43, no. 4, Oct. 2011.

[18] H. Zou, Y. Zhou, J. Yang, W. Gu, L. Xie, and C. Spanos, "Freecount: Device-free crowd counting with commodity wifi," in *Proc. IEEE GLOBECOM*, 2017, pp. 1–6.

[19] Z. Guo, F. Xiao, B. Sheng, L. Sun, and S. Yu, "Twcc: a robust through-the-wall crowd counting system using ambient wifi signals," *IEEE Trans. Veh. Technol.*, vol. 71, no. 4, pp. 4198–4211, 2022.

[20] F. Wang, F. Zhang, C. Wu, B. Wang, and K. R. Liu, "Respiration tracking for people counting and recognition," *IEEE Internet Things J.*, vol. 7, no. 6, pp. 5233–5245, 2020.

[21] T. Xin, B. Guo, Z. Wang, P. Wang, J. C. K. Lam, V. Li, and Z. Yu, "Freesense: A robust approach for indoor human detection using wi-fi signals," *Proc. ACM Interact. Mob. Wearable Ubiquitous Technol. (UbiComp)*, vol. 2, no. 3, pp. 1–23, 2018.

[22] H. Wang, D. Zhang, J. Ma, Y. Wang, Y. Wang, D. Wu, T. Gu, and B. Xie, "Human respiration detection with commodity wifi devices: Do user location and body orientation matter?" in *Proc. ACM Interact. Mob. Wearable Ubiquitous Technol. (UbiComp)*, 2016, pp. 25–36.

[23] D. Zhang, F. Zhang, D. Wu, J. Xiong, and K. Niu, "Fresnel zone based theories for contactless sensing," in *Contactless Human Activity Analysis*. Springer, 2021, pp. 145–164.

[24] M. J. Bocus, W. Li, J. Paulavicius, R. McConville, R. Santos-Rodriguez, K. Chetty, and R. Piechocki, "Translation resilient opportunistic wifi sensing," in *Proc. Int. Conf. Pattern Recognit. (ICPR)*, 2021, pp. 5627–5633.

[25] B. Xie, M. Cui, D. Ganesan, and J. Xiong, "Wall matters: Rethinking the effect of wall for wireless sensing," *Proc. ACM Interact. Mob. Wearable Ubiquitous Technol. (UbiComp)*, vol. 7, no. 4, pp. 1–22, 2024.

[26] W. Li, R. Gao, J. Xiong, J. Zhou, L. Wang, X. Mao, E. Yi, and D. Zhang, "Wifi-csi difference paradigm: Achieving efficient doppler speed estimation for passive tracking," *Proc. ACM Interact. Mob. Wearable Ubiquitous Technol. (UbiComp)*, vol. 8, no. 2, May 2024.

[27] W. Ge, Y. Tian, X. Liu, X. Tong, W. Qu, Z. Zhong, and H. Chen, "Crosstrack: Device-free cross-link tracking with commodity wi-fi," *IEEE Internet Things J.*, vol. 10, no. 20, pp. 18 028–18 041, 2023.

[28] M. Cominelli, F. Gringoli, and R. L. Cigno, "Passive device-free multi-point csi localization and its obfuscation with randomized filtering," in *Proc. MedComNet*, 2021, pp. 1–8.

[29] E. Gönültaş, E. Lei, J. Langerman, H. Huang, and C. Studer, "Csi-based multi-antenna and multi-point indoor positioning using probability fusion," *IEEE Trans. Wireless Commun.*, vol. 21, no. 4, pp. 2162–2176, 2022.

[30] G. Lim, B. Oh, D. Kim, and K.-A. Toh, "Human activity recognition via score level fusion of wi-fi csi signals," *Sensors*, vol. 23, no. 16, 2023.

[31] Y. Wang, J. Liu, Y. Chen, M. Gruteser, J. Yang, and H. Liu, "E-eyes: device-free location-oriented activity identification using fine-grained wifi signatures," in *Proc. ACM Int. Conf. Mobile Comput. Netw. (MobiCom)*, 2014, pp. 617–628.

[32] H. D. Hristov, *Fresnal Zones in Wireless Links, Zone Plate Lenses and Antennas*. Artech House, Inc., 2000.

[33] A. F. Molisch, *Wireless communications*. John Wiley & Sons, 2012, vol. 34.

[34] H. T. Friis, "A note on a simple transmission formula," *Proc. IRE*, vol. 34, no. 5, pp. 254–256, 1946.

[35] A. Kamann, P. Held, F. Perras, P. Zaumseil, T. Brandmeier, and U. T. Schwarz, "Automotive radar multipath propagation in uncertain environments," in *Proc. IEEE Intell. Transp. Syst. Conf.*, 2018, pp. 859–864.

[36] M. Dunna, C. Zhang, D. Sievenpiper, and D. Bharadia, "Scattermimo: Enabling virtual mimo with smart surfaces," in *Proc. ACM Int. Conf. Mobile Comput. Netw. (MobiCom)*, 2020, pp. 1–14.

[37] Z. Peng, L. Li, M. Wang, Z. Zhang, Q. Liu, Y. Liu, and R. Liu, "An effective coverage scheme with passive-reflectors for urban millimeter-wave communication," *IEEE Antennas Wireless Propag. Lett.*, vol. 15, pp. 398–401, 2015.

[38] F. Gringoli, M. Schulz, J. Link, and M. Hollick, "Free your csi: A channel state information extraction platform for modern wi-fi chipsets," in *Proc. ACM Int. Workshop Wirel. Netw. Testbeds Exp. Eval. Characterization (WiNTECH)*, 2019, pp. 21–28.

[39] D. Halperin, W. Hu, A. Sheth, and D. Wetherall, "Tool release: Gathering 802.11n traces with channel state information," *SIGCOMM Comput. Commun. Rev.*, vol. 41, no. 1, p. 53, Jan. 2011.

[40] J. Schäfer, B. R. Barrsiwal, M. Kokhkharova, H. Adil, and J. Liebehenschel, "Human activity recognition using csi information with nexmon," *Appl. Sci.*, vol. 11, no. 19, p. 8860, 2021.

[41] J. Hu, T. Zheng, Z. Chen, H. Wang, and J. Luo, "Muse-fi: Contactless muti-person sensing exploiting near-field wi-fi channel variation," in *Proc. ACM Int. Conf. Mobile Comput. Netw. (MobiCom)*, 2023, pp. 1–15.

[42] S.-H. Jeong, K. S. Shin, J. Park, S. Jo, and Y.-J. Suh, "Ubigest: Smartphone-based ubiquitous gesture recognition with wi-fi," *IEEE Internet Things J.*, 2024.

[43] Y. Li, D. Wu, J. Zhang, X. Xu, Y. Xie, T. Gu, and D. Zhang, "Diversense: Maximizing wi-fi sensing range leveraging signal diversity," *Proc. ACM Interact. Mob. Wearable Ubiquitous Technol. (UbiComp)*, vol. 6, no. 2, pp. 1–28, 2022.

[44] Z. Gao, Y. Gao, S. Wang, D. Li, and Y. Xu, "Crisloc: Reconstructable csi fingerprinting for indoor smartphone localization," *IEEE Internet Things J.*, vol. 8, no. 5, pp. 3422–3437, 2020.

[45] W. Wang, A. X. Liu, M. Shahzad, K. Ling, and S. Lu, "Understanding and modeling of wifi signal based human activity recognition," in *Proc. ACM Int. Conf. Mobile Comput. Netw. (MobiCom)*, 2015, pp. 65–76.

[46] X. Yang, S. Wu, M. Zhou, L. Xie, J. Wang, and W. He, "Indoor through-the-wall passive human target detection with wifi," in *Proc. IEEE Globecom Workshops (GC Wkshps)*, 2019, pp. 1–6.

[47] W. Wang, A. X. Liu, M. Shahzad, K. Ling, and S. Lu, "Device-free human activity recognition using commercial wifi devices," *IEEE J. Sel. Areas Commun.*, vol. 35, no. 5, pp. 1118–1131, 2017.

[48] R. W. Schafer, "What is a savitzky-golay filter? [lecture notes]," *IEEE Signal Process. Mag.*, vol. 28, no. 4, pp. 111–117, 2011.